[Article] www.whxb.pku.edu.cn

Pt/γ-Al_2O_3/$Ce_xZr_{1-x}O_2$ 催化剂低温催化燃烧去除饮食油烟

王健礼 王康才 曹红岩 陈永东 刘志敏
朱 艺 龚茂初 陈耀强*
(四川大学化学学院教育部绿色化学与技术重点实验室, 成都 610064)

摘要: 以 $Ce_xZr_{1-x}O_2$ 固溶体做载体, 制备了系列 Pt/γ-Al_2O_3/$Ce_xZr_{1-x}O_2$ 催化剂(x=1, 0.75, 0.5, 0.25, 0). 应用 Brunauer-Emmet-Teller (BET)比表面积分析、X 射线衍射(XRD)和 H_2 程序升温还原(H_2-TPR)等手段对催化剂进行相关表征, 并系统研究了催化剂在饮食油烟催化燃烧中的催化活性. BET 结果表明催化剂的比表面积随 Ce/Zr 摩尔比的减小而减小. XRD 结果表明贵金属 Pt 很好地分散在氧化铝和 $Ce_xZr_{1-x}O_2$ 固溶体上. H_2-TPR 结果发现催化剂 Pt/γ-Al_2O_3/$Ce_{0.5}Zr_{0.5}O_2$ 的还原峰面积最大且氧离子的流动性最好. 催化活性研究结果表明 Pt 负载在 $Ce_xZr_{1-x}O_2$ 固溶体上有利于油烟的催化燃烧, 降低了反应温度. 随着 $Ce_xZr_{1-x}O_2$ 固溶体中 Ce/Zr 摩尔比的变化, 催化剂的活性顺序为 Pt/γ-Al_2O_3/$Ce_{0.5}Zr_{0.5}O_2$>Pt/γ-Al_2O_3/$Ce_{0.25}Zr_{0.75}O_2$>Pt/γ-Al_2O_3/$Ce_{0.75}Zr_{0.25}O_2$>Pt/γ-Al_2O_3/CeO_2>Pt/γ-Al_2O_3/ZrO_2.

关键词: 饮食油烟; 催化燃烧; 储氧材料; 整体式催化剂
中图分类号: O643

Low Temperature Catalytic Combustion of Cooking Fume over Pt/γ-Al_2O_3/$Ce_xZr_{1-x}O_2$ Catalyst

WANG Jian-Li WANG Kang-Cai CAO Hong-Yan CHEN Yong-Dong
LIU Zhi-Min ZHU Yi GONG Mao-Chu CHEN Yao-Qiang*
(*Key Laboratory of Green Chemistry & Technology of the Ministry of Education, College of Chemistry, Sichuan University, Chengdu 610064, P. R. China*)

Abstract: Pt/γ-Al_2O_3/$Ce_xZr_{1-x}O_2$ (x=1, 0.75, 0.5, 0.25, 0) catalysts were prepared using $Ce_xZr_{1-x}O_2$ solid solution as support. The prepared catalysts were characterized by Brunauer-Emmet-Teller (BET) specific surface area analysis, X-ray diffraction (XRD), and H_2-temperature programmed reduction (H_2-TPR). Catalytic performances for the catalytic combustion of cooking fume were systematically investigated. Gas adsorption measurements showed that the BET surface areas of the as-prepared catalysts decreased as the Ce/Zr molar ratio decreased in the $Ce_xZr_{1-x}O_2$ solid solution. XRD results indicated that deposited Pt was well dispersed on the $Ce_xZr_{1-x}O_2$ and γ-Al_2O_3 matrix. H_2-TPR results revealed that the reduction peak area of Pt/γ-Al_2O_3/$Ce_{0.5}Zr_{0.5}O_2$ was the largest and that the oxygen mobility in this catalyst was noticeably promoted. It was found that the loaded Pt on the $Ce_xZr_{1-x}O_2$ solid solution lowered the reaction temperature, which was favorable for the catalytic combustion of cooking fume. The catalytic activity for the catalytic combustion of cooking fume changed with the variation of the Ce/Zr molar ratio in the $Ce_xZr_{1-x}O_2$ solid solution. The order of catalytic activity for catalytic combustion of cooking fume was: Pt/γ-Al_2O_3/$Ce_{0.5}Zr_{0.5}O_2$>Pt/γ-Al_2O_3/$Ce_{0.25}Zr_{0.75}O_2$>Pt/γ-Al_2O_3/$Ce_{0.75}Zr_{0.25}O_2$>Pt/γ-Al_2O_3/CeO_2>Pt/γ-Al_2O_3/ZrO_2.

Key Words: Cooking fume; Catalytic combustion; Oxygen storage material; Monolithic catalyst

Cooking fume is one of the three major pollution sources nowadays. It has been established that the pollutants in the cooking

Received: September 19, 2008; Revised: November 13, 2008; Published on Web: January 13, 2009.
*Corresponding author. Email: nic7501@email.scu.edu.cn; Tel/Fax: +8628-85418451.
国家自然科学基金(20773090)资助项目

fumes could do great harm to environment and human health[1–3]. With the quick development of restaurants in China, the cooking fume pollution becomes more and more serious. Due to the complexity of its components, cooking fume is notoriously difficult to be removed using static method. Conventional approaches to remove cooking fumes involve filtration of the fumes by water scrubbers, various types of filers, adsorption or washing. However, these methods are inefficient for abatement of particulate emissions, particularly in applications where the volume of particulate emissions is high. Thermal oxidation is also an option, but the expensive equipment, high operation and maintenance cost, and the production of toxic NO_x will offset the benefits of organics removal[4]. In this regard, catalytic combustion exhibits some advantages over the above-mentioned methods to convert the component of cooking fume to carbon dioxides and water[5–8]. For example, catalytic combustion could work at much lower temperatures and avoid the formation of toxic NO_x. To enhance high performance of the catalyst, catalyst is usually deposited on a monolithic substrate (known as cordierite honeycomb)[9,10]. Catalytic afterburners based on ceramic monoliths of long strait channels with three-way noble metal catalyst have become a worldwide standard[11]. Their outstanding performances are due to high specific area (4000 $m^2 \cdot m^{-3}$) and low pressure drop. Especially comparing to pack beds, monolithic catalyst exhibits excellent mechanism and thermal resistance.

CeO_2-ZrO_2 solid solution is one of the most important commercial catalytic supports and has been widely used in three-way automobile catalysts[12]. This material has been investigated since the early 1990s and is generally known that the incorporation of zirconium into the ceria lattice creates a high concentration of defects, thus improving the O^{2-} mobility in the lattice[13]. It possesses a large oxygen storage capacity (OSC) *via* a facile $Ce^{4+} \leftrightarrow Ce^{3+}$ redox process, and shows excellent ability to promote the dispersion of noble metals[14,15]. However, few reports about catalytic combustion of cooking fume on Pt/γ-Al_2O_3/$Ce_xZr_{1-x}O_2$ catalyst are known.

In this article, we present the optimization preparation of Pt/γ-Al_2O_3/$Ce_xZr_{1-x}O_2$ catalysts and the bench scale test of these catalysts in honeycomb type. The catalytic combustion of cooking fume over these catalysts was studied and the effect of different Ce/Zr molar ratios on the catalytic performance was systematically investigated. Some characterizations, such as XRD, TPR, and BET analyses, were also carried out to explain their different catalytic behaviors.

1 Experimental

1.1 Catalyst preparation

All reagents of analytic grade were purchased from Chengdu Kelong Chemical Reagents Factory. Deionized water was used throughout the experiments.

The $Ce_xZr_{1-x}O_2$ (x=1, 0.75, 0.5, 0.25, 0) solid solution was prepared by coprecipitation method. $Ce(NO_3)_3$ and $ZrOCO_3$ with a nominal composition were dissolved in an aqueous solution; then $NH_3 \cdot H_2O$ and $(NH_4)_2CO_3$ mixed aqueous solution was added under constant stirring and the resulting precipitate was filtered, washed with distilled water until no pH change could be detected, then calcined in air at 873 K for 4 h in a muffle furnace.

The Pt/γ-Al_2O_3 catalyst powder was prepared by impregnating γ-Al_2O_3 (S_{BET}=151.8 $m^2 \cdot g^{-1}$) with an aqueous solution of H_2PtCl_6. The resulting powders were dried at 383 K for 2 h and annealed at 773 K for 2 h, thus formed Pt/γ-Al_2O_3 with w(Pt)=0.4% (powder A).

H_2PtCl_6 solution was deposited on $Ce_xZr_{1-x}O_2$ powders by immerse method. The resulting powders were dried at 383 K for 2 h, then calcined at 773 K for 2 h, thus forming Pt/$Ce_xZr_{1-x}O_2$ with w(Pt)=0.4% (powder B).

The powders A and B were blended in a mass ratio of 1∶1, and H_2O was added, ground and slurry was formed. The slurry was wash-coated on the monolithic substrate (62 cell·cm^{-2}), then dried at 393 K for 2 h and calcined at 773 K for 3 h. The noble metal content of all catalysts was 0.5 g·L^{-1}. Pt loaded on γ-Al_2O_3/CeO_2, γ-Al_2O_3/$Ce_{0.75}Zr_{0.25}O_2$, γ-Al_2O_3/$Ce_{0.5}Zr_{0.5}O_2$, γ-Al_2O_3/$Ce_{0.25}Zr_{0.75}O_2$, γ-Al_2O_3/ZrO_2, γ-Al_2O_3, and $Ce_{0.5}Zr_{0.5}O_2$ was designed as T1, T2, T3, T4, T5, T6, and T7, respectively.

1.2 Catalyst characterization

Surface area of Pt/γ-Al_2O_3/$Ce_xZr_{1-x}O_2$ was determined by the Brunauer-Emmet-Teller (BET) method using Autosorb-ZXF-05 (Xibei Chemical Institute, China). The sample was degassed for 3 h at 623 K, and then cooled to 77 K using liquid N_2 at which point N_2 adsorption was measured.

Total oxygen storage capacity (OSC) was measured by oxygen pulse method. Prior to measurement, the sample (200 mg) was reduced at 823 K under H_2 flow (40 mL·min^{-1}) for 45 min and cooled down to 473 K under N_2 flow (40 mL·min^{-1}), and then pulse of oxygen (82 μmol·g^{-1} sample) was injected up to the breakthrough point. OSC was evaluated from oxygen consumption.

X-ray diffraction (XRD) data were collected on a DX-1000 X-ray diffractometer with Cu K_α radiation (λ=0.15418 nm) and graphite filter. The X-ray tube was operated at 45 kV and 25 mA. Samples were scanned in the 2θ range from 10° to 90°. The X-ray diffraction line positions were determined with a step size of 0.03°.

H_2-temperature programmed reduction (H_2-TPR) experiments were carried out in a conventional system equipped with a thermal conductivity detector. All samples (100 mg) were pretreated in a quartz U-tube in a flow of pure N_2 (20 mL·min^{-1}) at 723 K for 1 h, and then cooled down to 300 K. The reduction was carried out in a flow of 5% H_2-N_2 (20 mL·min^{-1}) mix gas from 300 to 1050 K under a linear heating rate of 10 K·min^{-1} and the amount of hydrogen consumed was determined by a thermal conductivity detector (TCD).

1.3 Activity measurement

The activity measurements were carried out in a conventional fixed-bed flow reactor. Schematic setup of the equipment was shown in Fig.1. Pressed air (with oxygen partial pressure around 0.1 MPa) pumped into a three-neck bottle, which was filled with

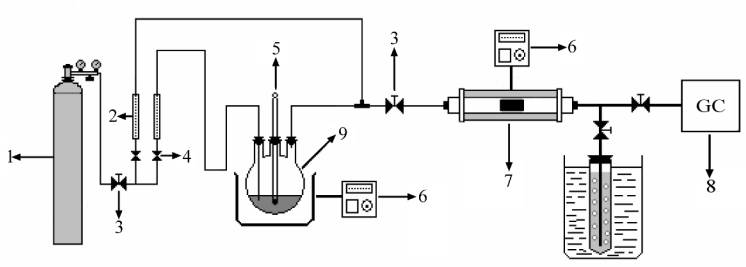

Fig.1 Experimental set-up used for the catalytic combustion experiment

(1) air cylinder, (2) rotameter, (3) control valve, (4) switch valve, (5) thermometer, (6) temperature control system, (7) reactor, (8) gas chromatograph, (9) three-neck bottle

commercial sunflower cooking oil. The flask was sealed with only inlet for pumped air and outlet for fume brought by air. A thermal meter was inserted under oil surface to monitor the temperature. The desired flow-rate was maintained by a flow meter.

The cooking oil fume was feed by heating the oil to 553 K in a fume heater controlled by a CN 76030 heat controller (Omega). The effluent from this process was introduced to a small column reactor whose temperature was controlled by a CN 76030 heat controller and monitored using platinum RTD probes (Omega) and the probes demonstrated that the reactor was isothermal. To prevent oil fume condensation, all the connecting pipes were stainless and were wrapped with the heating belt to keep temperature around 443 K. The small column reactor was packed with catalyst. The gas hourly space velocity (GHSV) of cooking fume was controlled by adjusting the flow rate of the pressed air into the heated oil.

The gaseous products were analyzed by using on-line gas chromatograph (GC-2000II) with a Porapak T column and thermal conductivity detector (TCD).

The cooking oil fumes effluent from the small column reactor were collected in an impinger filled with 100 mL CCl_4 for 10 min continuously and the oil concentrations were measured using a JDS106-A oil infrared oil meter (Ji Lin Beiguang Inc.).

2 Results and discussion

2.1 Textural and OSC properties

The surface areas of the catalysts were determined by N_2 adsorption experiments. The effect of different Zr/Ce molar ratios on the surface area is clearly showed in Table 1. T1 without ZrO_2 composition has the highest surface area (ca 105.2 $m^2 \cdot g^{-1}$). The substitution of cerium by an increasing amount of zirconium decreases their surface areas, which are ca 102.7, 99.6, and 87.5 $m^2 \cdot g^{-1}$ for T2, T3, and T4 samples, respectively. For T5 sample without CeO_2 composition, the observed surface area is the lowest (ca 60.1 $m^2 \cdot g^{-1}$). Among these five catalysts, T3 has the largest pore volume (ca 0.25 $cm^3 \cdot g^{-1}$) and pore size (ca 4.223 nm).

Table 1 Surface parameters and OSCs of the catalysts

Catalyst	S_{BET}/($m^2 \cdot g^{-1}$)	V_{pore}/($cm^3 \cdot g^{-1}$)	d_{pore}/nm	Oxygen consumption ($\mu mol \cdot g^{-1}$)
T1	105.2	0.19	3.448	210.5
T2	102.7	0.22	3.567	501.9
T3	99.6	0.25	4.223	532.7
T4	87.5	0.24	3.934	519.1
T5	60.1	0.23	3.636	0.0

The different Zr/Ce molar ratios in the catalysts also affect their OSC properties, which are evaluated by the oxygen consumption. As seen in Table 1, the oxygen consumption increased with increasing ZrO_2 content to a maximum (532.7 $\mu mol \cdot g^{-1}$) when Zr/Ce molar ratio is 1.0, above which the oxygen consumption dropped. It is well known that the OSC property is closely related to the $Ce^{4+} \leftrightarrow Ce^{3+}$ redox process. As expected, T5 sample without CeO_2 composition exhibits no OSC property.

2.2 XRD characterization

The X-ray diffraction patterns of the as-synthesized catalysts are shown in Fig.2. The T1 sample shows well-defined peaks corresponding to a cubic fluorite structure and γ-Al_2O_3 phase. The most intense diffraction peak of $Ce_{0.75}Zr_{0.25}O_2$, $Ce_{0.5}Zr_{0.5}O_2$, and $Ce_{0.25}Zr_{0.75}O_2$ slightly shifts to higher diffraction angles, which could be attributed to the shrinkage of lattice due to the replacement of Ce^{4+} with a smaller Zr^{4+} cation radius. The diffractograms corresponding to $Ce_{0.75}Zr_{0.25}O_2$, $Ce_{0.5}Zr_{0.5}O_2$, and $Ce_{0.25}Zr_{0.75}O_2$ do not show any diffraction peaks assigned to zirconia as segregated phases. Based on these obsessions, it is clear that these mixed oxides are solid solutions. It should be noted here that T5 sample without CeO_2 component shows intense diffraction peaks corresponding to the monoclinic phase of ZrO_2. Of the five samples, the diffraction peaks of Pt are not detected by XRD, indicating that the deposited Pt is well dispersed on the $Ce_xZr_{1-x}O_2$ and γ-Al_2O_3 matrix.

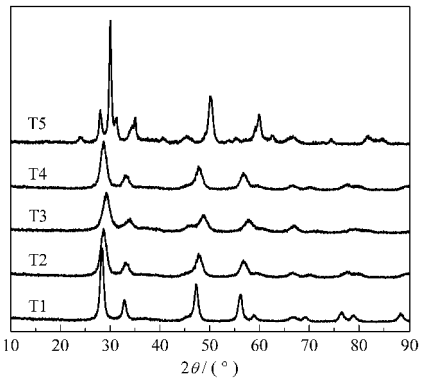

Fig.2 XRD patterns of Pt/γ-Al_2O_3/$Ce_xZr_{1-x}O_2$

Table 2 The average particle sizes of the catalysts

Catalyst	$D_{(111)}$/nm
T1	9.1
T2	6.0
T3	4.7
T4	5.4
T5	14.1

The average particle sizes of these samples were estimated from the width of principal diffraction peaks using the Scherrer equation: $D=0.92\lambda/B\cos\theta$, where D is the average particle size of the sample, λ is the wavelength of the radiation, θ is the diffraction angle, and B is the corrected half-width of the diffraction peak. The results of the average particle size are presented in Table 2. It is clear that the particle size decreases with increasing of ZrO_2 content to a minimum (4.7 nm) when Zr/Ce molar ratio is 1.0, above which particle size increases gradually. The increased particle size would lead to the sharp decrease of BET surface area, which is evidenced by the BET surface area analyses (x<0.5).

2.3 Temperature programmed reduction

Temperature programmed reduction has been widely used to characterize reductive property of ceria-based materials. Cerium oxide and PtO_2 are well known for their facile reducibility comparing with other fluorite-type oxides. The TPR profile of ceria shows a two-peak pattern, which indicates that the reduction of ceria may follow a two-step process. The peak present at 773 K is assigned to the reduction of the surface cerium oxide and PtO_2, while reduction of the bulk is proposed as the cause of the high-temperature signal at 1120 K. In contrast, the TPR profiles of the mixed oxides essentially show a main broad reduction feature, which is in agreement with the promotion of the reduction in the bulk of the mixed oxide upon doping with ZrO_2. Indeed, doping ZrO_2 into the cubic CeO_2 would result in the distortion of the cubic fluorite lattice, which is revealed by XRD analysis. As a consequent, reduction process is no longer confined to the surface but extended deep into the bulk. Fig.3 clearly shows the change of the reduction behavior of CeO_2 as main hydrogen consumption shifts to lower temperatures[16,17].

The reduction process of a cerium atom in a ceria-zirconia mixed oxide occurs according to the following equation:

$$Ce_xZr_{1-x}O_2+\delta H_2 \rightarrow Ce_xZr_{1-x}O_{2-\delta}+\delta H_2O+\delta V_O$$

Where the elimination of the capping oxygen anion as water molecules involves the appearance of an oxygen vacancy (V_O). The presence of those vacancies considerably promotes the mobility of oxygen from the bulk to the surface. Therefore, the area of peak is proportional to the amount of Ce^{3+} formed, and also is proportional to the amount of oxygen vacancies, which is relate to the oxygen mobility[18]. For T3, the reduction degree is the largest. The oxygen mobility in this catalyst is noticeably promoted, which is in good harmony with the catalytic activity, as discussed below.

2.4 Catalytic performance

Ignition or light-off curves are the most widespread way to evaluate the catalytic activity in cooking fume complete oxidation studies. These curves simply depict the cooking fume conversion *versus* reaction temperature. The conversion can be calculated by measuring the extent of cooking fume removal that takes place in the gaseous stream as reaction temperature increases. The activity of the series of $Pt/\gamma\text{-}Al_2O_3/Ce_xZr_{1-x}O_2$ catalyst in the catalytic combustion of cooking fume is plotted in Fig.4. These curves are frequently characterized by two parameters, T_{50} and T_{90}. T_{50} is the temperature at which conversion is 50% , and is often used as an indicator of relative activities of the catalysts; while T_{90} is the temperature at which conversion is 90% .

It can be seen from Fig.4 that the catalytic activity for the oxidation of cooking fume over T7 is quite low. The temperature at which the cooking fume conversion reached 50% (T_{50}) is 673 K. For T6, T_{50} is 560 K and T_{90} is 673 K. By the use of $\gamma\text{-}Al_2O_3$ and $Ce_xZr_{1-x}O_2$ as support, the catalytic activity could be greatly promoted. In general, the catalytic activity of $Pt/\gamma\text{-}Al_2O_3/Ce_xZr_{1-x}O_2$ ($1>x>0$) is better than that of T1 (x=1) and T5 (x=0). Compared with pure CeO_2 and ZrO_2, the presence of $Ce_xZr_{1-x}O_2$ ($1>x>0$) in the catalysts leads to a significant reduction in T_{50} by 30 to 70 K. The order of catalytic activity is T3 (479 K)> T4(500 K)> T2(510 K)> T1(549 K)> T5(559 K), the values in brackets are the corresponding T_{50} values.

The catalytic activities of mixed oxides are noticeably higher

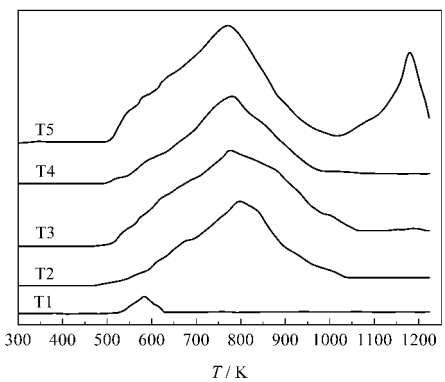

Fig.3 H_2-TPR profiles of $Pt/\gamma\text{-}Al_2O_3/Ce_xZr_{1-x}O_2$

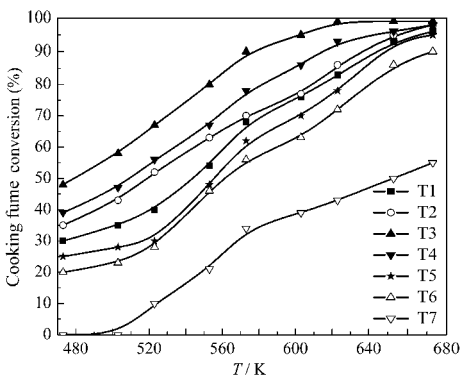

Fig.4 Light-off curves of cooking fume over catalysts

Table 3 T_{50} (K) values for the combustion of cooking fume in the presence or absence of oxygen

	T1	T2	T3	T4	T5
air	549	510	479	500	559
N_2	609	583	562	578	618

than that of pure ceria and pure zirconia. It can be speculated that Zr incorporated into CeO_2 lattice forms a solid solution influence the catalytic activity for cooking fume oxidation. Thus, the catalyst with an equimolar composition seems to be the most active mixed oxide for the abatement of cooking fume. This catalyst is appropriately associated with relatively accessible lattice oxygen species. As mentioned above, these structural changes are attributed to the incorporation of ZrO_2 into the CeO_2 lattice.

To further study the role of oxygen in the reaction, cooking fume destruction was also evaluated in the absence of oxygen by replacing flowing air with flowing nitrogen. Prior to the experimental run, the reaction environment was purged with nitrogen to remove traces of oxygen. Although reaction is still noticeable, catalytic activities in nitrogen is worse than that in air. The observed conversion in nitrogen is assigned to the involvement of oxygen species from the mixed oxide in the reaction mechanism, which diffuses from the bulk of catalyst to the surface[19,20]. Based on the different activity in different atmosphere, it can be speculated that oxygen from the gas-phase is needed to form electrophilic oxygen species, and therefore, catalyst can achieve high catalytic activity in air. T3 is the most active catalyst due to its excellent oxygen mobility as revealed by H_2-TPR.

Table 3 lists the T_{50} values of the combustion of the cooking fume under oxidizing (21% O_2/N_2) and inert (pure N_2) conditions. An eventual time-on-stream behavior of all catalysts at constant temperature under inert conditions would result in a gradual loss of activity due to the continuous participation of oxygen species.

Apart from the catalytic behavior of mixed oxides, the product distribution of combustion reaction was also analyzed. The CO_2 is the only gaseous product as detected by TCD.

3 Conclusions

The catalytic activities of a series of Pt/γ-Al_2O_3/$Ce_xZr_{1-x}O_2$ catalysts with varying Ce/Zr molar ratio have been evaluated for the combustion of cooking fume under dry conditions. The order of catalytic activity is Pt/γ-Al_2O_3/$Ce_{05}Zr_{05}O_2$>Pt/γ-Al_2O_3/$Ce_{0.25}Zr_{0.75}O_2$>Pt/γ-Al_2O_3/$Ce_{0.75}Zr_{025}O_2$>Pt/γ-Al_2O_3/CeO_2>Pt/γ-Al_2O_3/ZrO_2. Incorporation of ZrO_2 into the CeO_2 lattice noticeably decreases the reaction temperature and would favor the oxygen mobility in the solid solution, which is responsible for controlling the catalytic activity. The major combustion product is carbon dioxide. Further attention should be focused on the action atmosphere.

References

1 Hung, H. S.; Wu, W. J.; Cheng, Y. W.; Wu, T. C.; Chang, T. C.; Lee, H. *Mutat. Res.-Gen. Tox. En.*, **2007, 628**: 107

2 Chang, Y. C.; Li, P. *Toxicol. Appl. Pharm.*, **2008, 228**: 76

3 Chiang, T. A.; Wu, P. F.; Liao, S. Y.; Wang, L. F.; Ko, Y. C. *Food Chem. Toxicol.*, **1999, 37**: 125

4 María, R. M.; Bibinan, P. B.; Luis, E. C. *Fuel*, **2008, 87**: 1177

5 Yuan, S. H.; Shen, M.; Gong, M. C.; Wang, J. L.; Yan, S. H.; Cao, H. Y.; Chen, Y. Q. *Acta Phys. -Chim. Sin.*, **2008, 24**: 364 [袁书华, 沈 美, 龚茂初, 王健礼, 闫生辉, 曹红岩, 陈耀强. 物理化学学报, **2008, 24**: 364]

6 Yang, Y. X.; Xu, X. L.; Sun, K. P. *Catal. Commun.*, **2006, 7**: 756

7 Garin, F. *Catal. Today*, **2004, 89**: 255

8 Yang, J.; Jia, P.; Wang, Y.; You, W. *Appl. Catal. B-Environ.*, **2005, 58**: 123

9 Irusia, S.; Pina, M. P.; Menéndez, M.; Samamaría, J. *J. Catal.*, **1998, 179**: 400

10 Haruta, M.; Ueda, A.; Tsubota, S.; Sanchez, R. M. T. *Catal. Today*, **1996, 29**: 443

11 Williams, J. L. *Catal. Today*, **2001, 69**: 3

12 Fornasiero, P.; Di Monte, R.;Rao, G. R.; Kašpar, J.; Meriani, S.; Trovarelli, A.; Graziani, M. *J. Catal.*, **1995, 151**: 168

13 Nagai, Y.; Yamamoto, T.; Tanaka, T.; Yoshida, S.; Nonaka, T.; Okamoto, T.; Suda, A.; Sugiura, M. *Catal. Today*, **2002, 74**: 225

14 He, H.; Dai, H. X.; Wong, K. W.; Au, C. T. *Appl. Catal. A-Gen*., **2003, 251**: 61

15 He, H.; Dai, H. X.; Au, C. T. *Catal. Today*, **2004, 90**: 245

16 Boaro, M.; Vicario, M.; Leitenburg, C.; Dolcetti, G.; Trovarelli, A. *Catal. Today*, **2003, 77**: 407

17 Leitenburg, C.; Trovarelli, A.; Llorca, J.; Cavani, F.; Bini, G. *Appl. Catal. A-Gen.*, **1996, 139**: 161

18 Balducci, G.; Kašpar, J.; Fornasiero, P.; Graziani, M.; Islam, M. S.; Gale, J. D. *J. Phys. Chem. B*, **1997, 101**: 1750

19 Ozawa, M.; Loong, C. K. *Catal. Today*, **1999, 50**: 329

20 Kozlov, A. I.; Kim, D. H.; Yezerets, A.; Andersen, P.; Kung, H. H.; Kung, M. C. *J. Catal.*, **2002**, **209**: 417